Article:
Dhimish, Mahmoud and Mather, Peter (2019) Development of Novel Solar Cell Micro Crack Detection Technique. IEEE Transactions on Semiconductor Manufacturing. pp. 277-285. ISSN 0894-6507

https://doi.org/10.1109/TSM.2019.2921951

Development of Novel Solar Cell Micro Crack Detection Technique

Mahmoud Dhimish, ***Member, IEEE***, Peter Mather, ***Member, IEEE***

***Abstract*— This paper presents the development of a solar cell inspection manufacturing execution system (MES). The main objective of the MES is to detect micro cracks in the manufacturing process of solar cells. Hence, to accept or reject a solar cell during the assembling unit. The proposed MES consists of three stages, at first stage, the inspection system will be placed on the manufacturing process of the solar cell. After the solar cell has been manufactured, it will pass under an in-line electroluminescent (EL) system. At this stage, an OR operation between a healthy/no-crack and the inspected solar cell image will be obtained. This OR operation will generate a better calibration for the cracks in the PV solar cell image. The final calibrated image presents a high quality, and low noise structure, thus easier to identify the micro cracks size, location and orientation. The last stage evaluates the calibrated image using the plot profile which is well known as the distance in pixels vs. the gray level of the image. The plot profile will indicate whether to accept or reject the solar cell, 10% confidence interval for the gray level was used to identify the upper and lower detection limits.**

Index Terms*— *Photovoltaic; Solar cells; Micro cracks; Electroluminescence.

I. INTRODUCTION

Micro cracks in solar cells are a common issue for Photovoltaic (PV) solar cells manufacturing systems. They are unlikely to avoid and, so far, the impact of solar cells' micro cracks has been reported with limited understanding how they behavior and in what extent the cracks should be accepted, and their impact could be considered as negligible.

Several state-of-the-arts methods have been proposed widely in order to detect solar cells micro cracks; resonance ultrasonic vibrations (RUV) method for crack detection in PV silicon wafers has been firstly proposed by [1] and [2]. This detection method uses ultrasonic waves of a plausible frequency though a transducer operating on a range of 20 to 90 kHz. The transducer consists of core unit which allows the vacuum to couple between the solar cell wafer and transducer by applying nearly 40-kPa pressure to the backside of the wafer. This method is sensitive to the crack orientation, size and length, and can only be used to reject/accept solar cells wafers. Nevertheless, it does not feature the exact location/area of the affected solar cell.

Photoluminescence (PL) detection method was firstly eveloped to enhance the detection of solar cells micro cracks. This technique can be used to detect micro cracks in silicon wafers as well as in large-scale PV panels [3]. PL technique could be cast-off not only at the end of the production process of solar cells but also it is commonly situated in the interior process of production line [4]. Authors in [5] developed a novel PL system that allows inhomogeneous radiation of light in order to enhance the detection of solar cells micro cracks. The results show that the usage of inhomogeneous illumination suggestively ranges the possibility of photoluminescence imaging applications for the classification of solar cells cracks detection. On the other hand, most recently, the PL images were acquired using the sun as an individual source of illumination. This is done using an appropriate optical filtering processing unit that extends the operation of solar cells at their optimum test condition scenarios [6]. While the main advantage of this technique that it enables the detection of solar cells micro cracks including point/dot and line cracks.

Another predominantly used method to detection solar cells micro cracks is the Electroluminescence (EL). This method is the form of luminescence in which electrons are excited into the conduction band using electrical current by connecting the inspected solar cell in forward biasing mode [7]. This method is frequently used since it can be applied not only on small small-scale solar cell sizes but also with full-scale PV panels [8]. In principle, the EL technique necessitates the inspected solar cell to be in the forward bias condition in order to yield infrared radiation, resulting an EL waves that varies from 950 to 1250 nm. Emission peak intensity is reliant on the compactness of defects in the solar cell, with less defects resulting in extra emitted EL waves [9]. The EL setup would be preferable to be placed in a dark room to eliminate the interaction between EL waves and any other source of light. In addition, the image of the cells cracks is typically taken by cooled charge-coupled device (CCD) camera; the configuration and construction of the EL setup is accessible in [10]. In a CCD image sensor, pixels are represented by p-doped metal-oxide-semiconductors (MOS) capacitors. The capacitors are biased above the threshold for inversion when image acquisition begins, allowing the conversion of incoming photons into electron charges at the semiconductor-oxide interface; the CCD is then used to read out these charges. Although CCD are not the only technology to allow for light detection, but they are widely used in professional, medical, and scientific applications where high-quality image data are required.

M. Kontges *et al.* [11] examined the impact of solar cells micro cracks using the conventional EL imaging technique. The outcome of the analyses proves that micro cracks could decrease the output power of a solar cells by more than 2.5%. Furthermore, the orientational distribution of solar cells micro cracks was firstly obtainable by S. Kajari-Schröder *et al.* [12]. The micro cracks were categorized into six sub-categories including dendritic, -45°, +45°, several, perpendicular to busbars and parallel to busbars. The analysis has been carried out using 27 different PV panels, where the maximum micro cracks are associated with parallel to busbars with 50% comparative occurrence.

Mahmoud Dhimish and Peter Mather are with the Department of Engineering and Technology, Laboratory of Photovoltaics, University of Huddersfield, HD1 3DH, United Kingdom (e-mail: M.A.Dhimish@hud.ac.uk; P.mather@hud.ac.uk).

The biggest disadvantage of EL imaging systems that they require a large-scale setup including a CCD camera and power supply [13]. Whereas the main advantage of this technology that it is considerable cheaper compared to other available cracks detection methods [14].

Other detection methods, such as infrared thermography (IRT) imaging is used detect abnormal conditions affecting PV modules, such as micro cracks. The IRT thermal imaging detects radiation in the long-infrared range of the electromagnetic spectrum (roughly from 9-14 μm), and produce images of that radiation, called thermograms.

According to [15], a suitable detection method, capable of detecting failure modes such as hot-spots and micro cracks in solar cells using an intelligent I-V kernel extreme learning machine method as well as using the IRT technique. While, [16] and [17], presented a novel thermal imaging technique using the IRT method to detect possible hot-spots and micro cracks in solar wafer, these techniques strongly depend on the thermal output image, while there are significant uncertainly in the data analysis due to the angle of detection, thermal camera accuracy, and some environmental conditions that might affect the resolution of the captured image such as partial shading conditions.

In this paper, EL imaging technique was used to capture the micro cracks in PV solar cells. The EL detection technique is already shown in our previous articles [7] and [18]. Furthermore, the main contribution of this work is illustrated as follows:

- **Technique selection:** comparing different techniques to analyses the difference between crack-free and cracked solar cells under the developed solar cell inspector manufacturing execution system (MES).
- **Image resolution:** finding the most appropriate method that has the finest output image arrangement, for PV solar cell micro cracks detection.
- **Evaluation:** the proposed micro crack detection and image enhancement technique will be evaluated using actual solar cell images and compared to previously published articles.
- **Plot profile:** the main challenge is to identify whether to accept or reject the solar cell in the manufacturing process. This was attainable using the plot profile of the final calibrated image by the value of the image gray level for the micro cracked solar cells.

II. Solar Cell Inspection System

The developed solar cell inspector manufacturing execution system (MES) is shown in Fig. 1. The inspector system consists of three stages which can be described as follows:

1. Solar cell manufacturing process: at this stage of the MES system, the solar cell already has been completely manufactured, whilst the inspection of the reliability and durability of the solar cell not yet confirmed within the international standards.
2. Solar cell inspector MES: after the solar cell is ready to be inspected, it will pass under an in-line solar cell inspector, in which it includes an electroluminescence system. The system is comprised of a light-tight black-box where housed inside is a digital camera and a sample holder. The digital camera is equipped with a standard F-mount 18–55 mm lens. To allow for detection in the near infrared, the IR filter was removed and replaced with a full spectrum window of equal optical path length. In our setup a Nikon D40 was used, but in principle any digital camera with similar grade CCD or CMOS sensor and where the IR filter can be removed would serve the purpose. The bias was applied and the resultant current and the voltage are measured by a voltage and current sensors which are connected to the personal computer (PC).
3. LabVIEW-based interface system: at this stage, the captured EL image of the solar cell will sent though a LabVIEW application in order to inspect and localize the micro cracks, therefore, to accept or reject the solar cell wafer. If the solar cell is accepted, it would be sent to the assembling unit; practically to assemble the solar cell as a large-scale PV module, whereas, if the solar cell is rejected, it will be recycled.

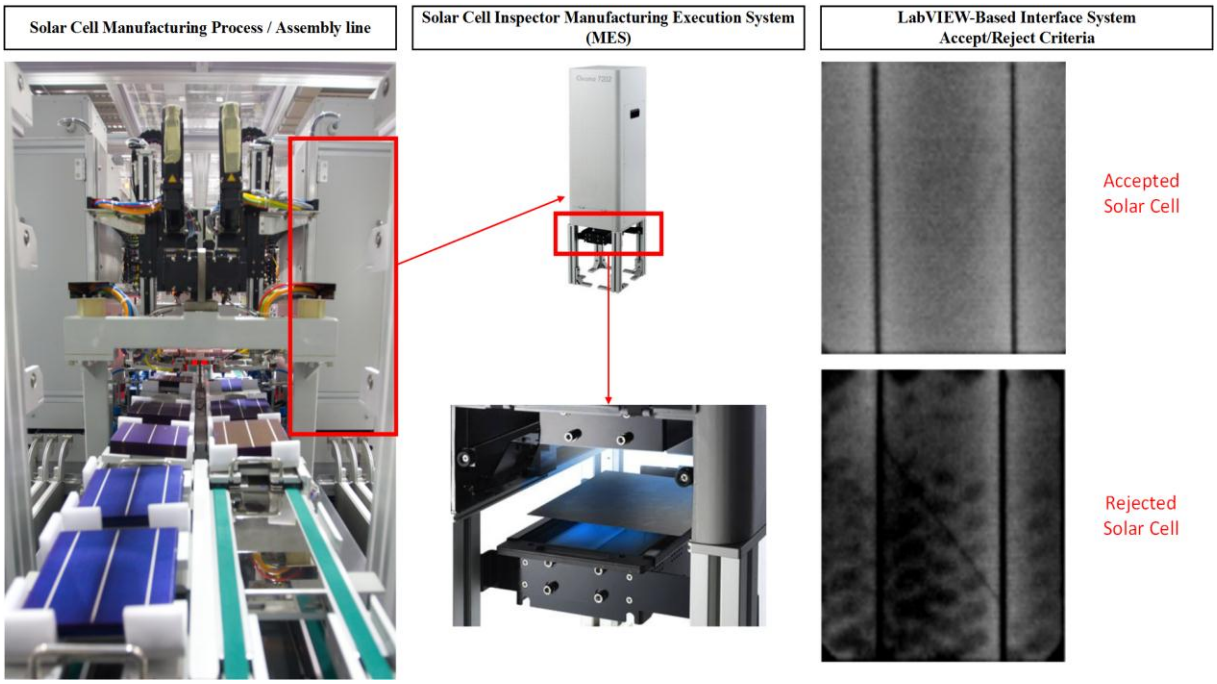

Fig. 1. Solar cell manufacturing and inspection system

III. Enhancing Solar Cell Micro Crack Inspection

This section discusses the appropriate level of selection for the proposed EL detection technique. Fig. 2 demonstrates the recombination of healthy vs. cracked solar cell samples. Six dissimilar methods are used to combine both images, initial using "OR" function, culmination with the subtraction method [19]-[25]. The output images for each method is also confirmed as shown in Fig. 2.

It is worth noting that the division method has a complete black output calibrated image, while the second-worst output image is when subtracting the cracked from the healthy solar cell image. Nevertheless, the optimum image for the crack identification is observed using the OR function (cracked solar cell image ORing with healthy solar cell image). This outcome is found because the crack-free image would not anticipate in an additional noise to the cracked solar cell image, though, it scrubs the parts of the image which have no micro cracks.

We have selected the OR function, since it provides the highest resolution and labels all cracks within the inspected solar cell sample; compared to other methods, which have limited resolution and cracks is hardly to be identified. In fact, each of the above listed techniques are based on a specific process which calculate bit-by-bit image pixels, thus remove the noise and improves the quality of the output cracked solar cell image, the process for 2 bits is described in Fig. 3(a). As a result, the detection technique leads for improved image structure. It is worth noting that the crack-free vs. cracked solar cell sample images are processed into binary signal using 200 x 200 pixel division process. Obtained bits are processed by an OR function in order to generate the output image of cracks in the observed solar cell samples.

Fig. 3(b) shows the output image of the cracked solar cell before and after the ORing bit-by-bit of the pixels for the observed image. The output image contains imperfect source of noise and the filtration process for the noisy areas have clearly disappeared.

In Fig. 3(b) two locations of the examined solar cell are labelled. Looking at the conventional EL image, the first area shows a long crack spread out in the solar cell. However, using the proposed OR function, the cracked area is more visible and fewer cracks are also present compared to the original EL image. Same remark is confirmed for the second area shown in Fig. 3(b). In regards with this observation, it is obvious that the original EL image does contain a noisy figure of the cracks, while this noise could possibly be added by the CCD camera, but as a ultimate remark this is not a real damage in the solar cell which cannot be identified by the conventional EL imaging technique. It is worth noting that the healthy/crack-free solar cell image is fixed, pre-captured using the EL camera and fixed as reference to the comparison with an inspected cell.

On the other hand, we have tested two other solar cell samples using both the conventional EL imaging vs. the proposed detection method, testified in Figs. 3(c) and 3(d). It is well-observed that after using the proposed method the crack position, size and orientation is more visible. Resulting in an improved solar cells micro cracks identification process.

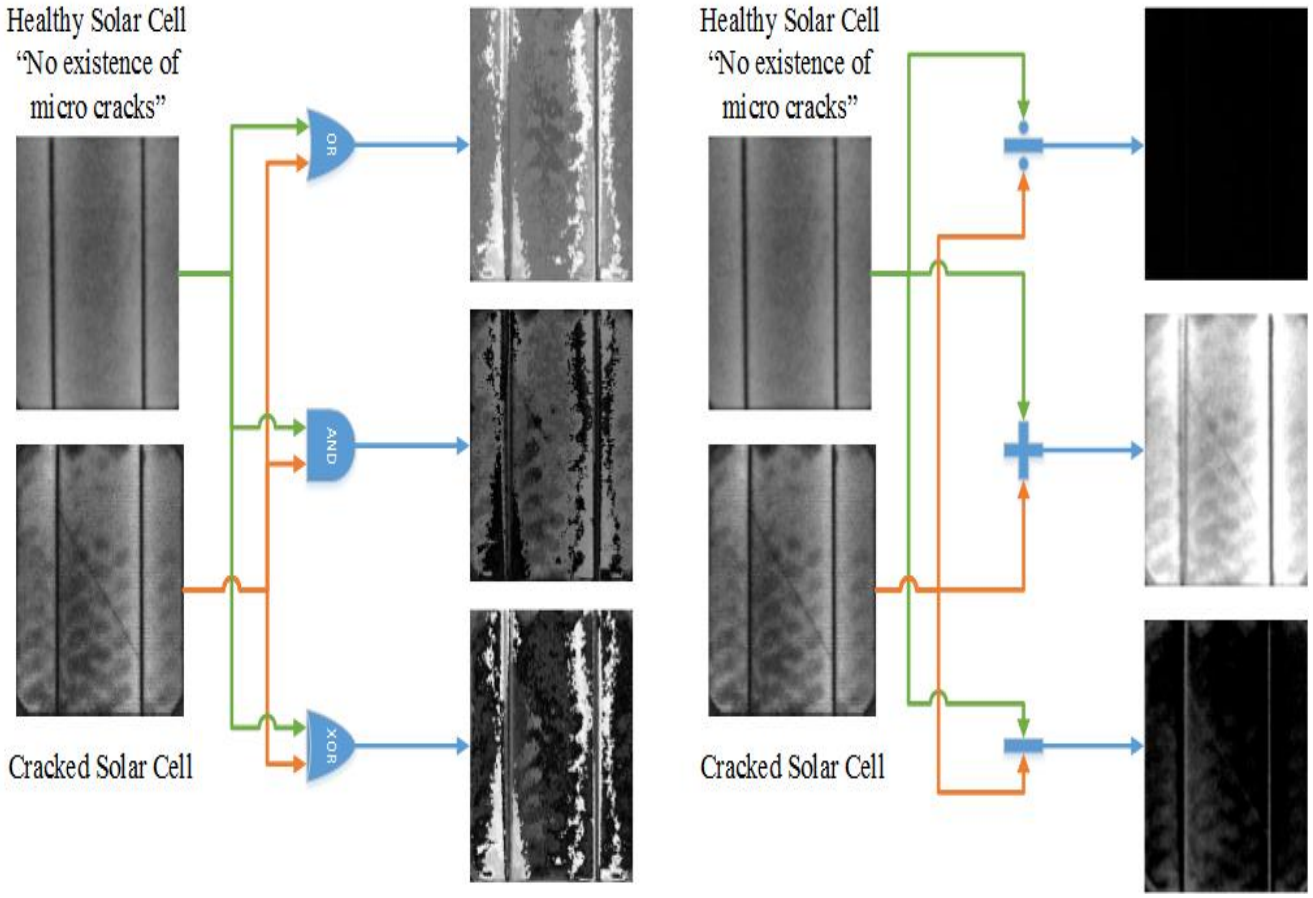

Fig. 2. The image of the healthy cell combined with cracked solar cell using various techniques (OR, AND, XOR, Division, Addition, Subtraction)

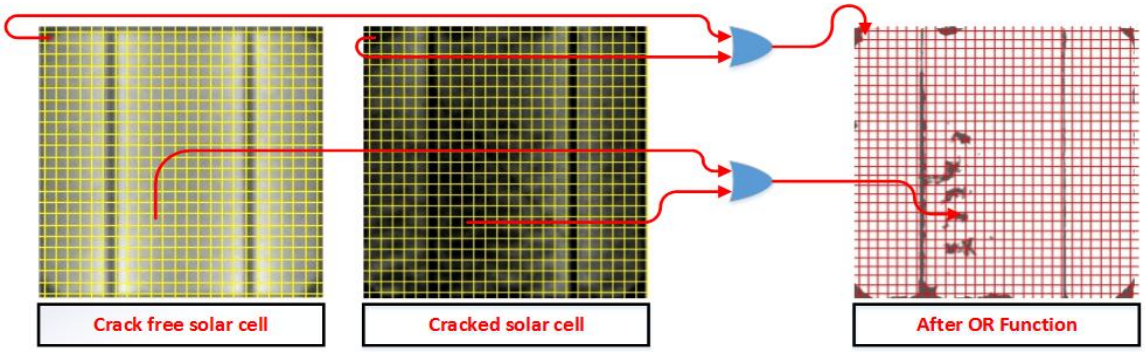

(a)

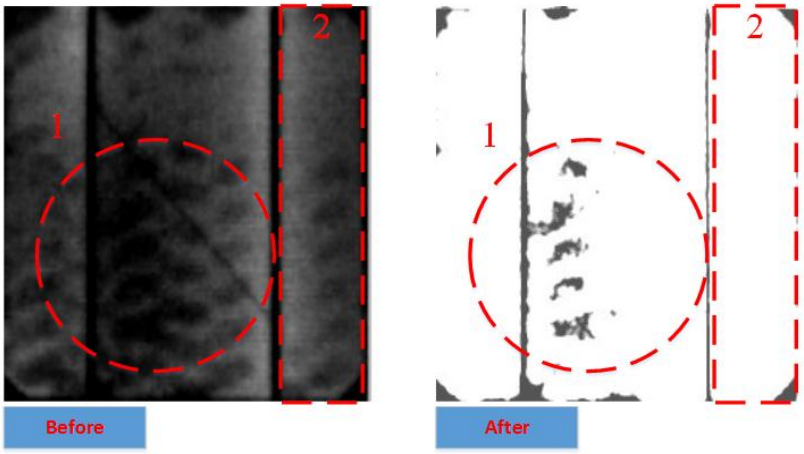

(b)

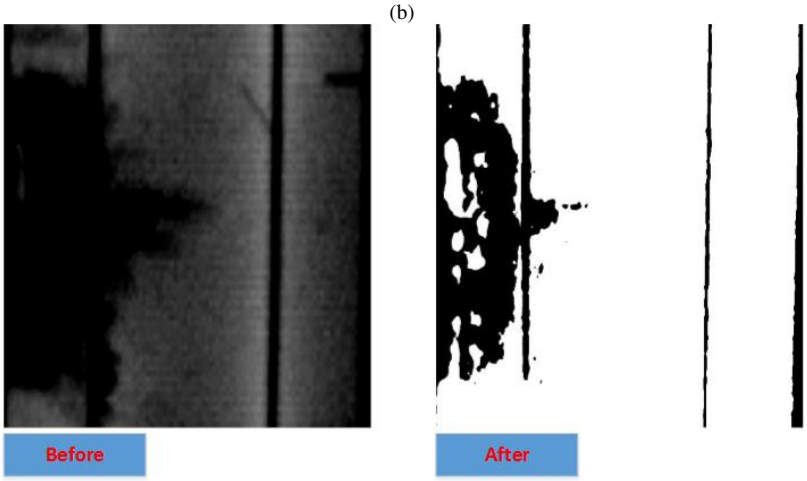

(c)

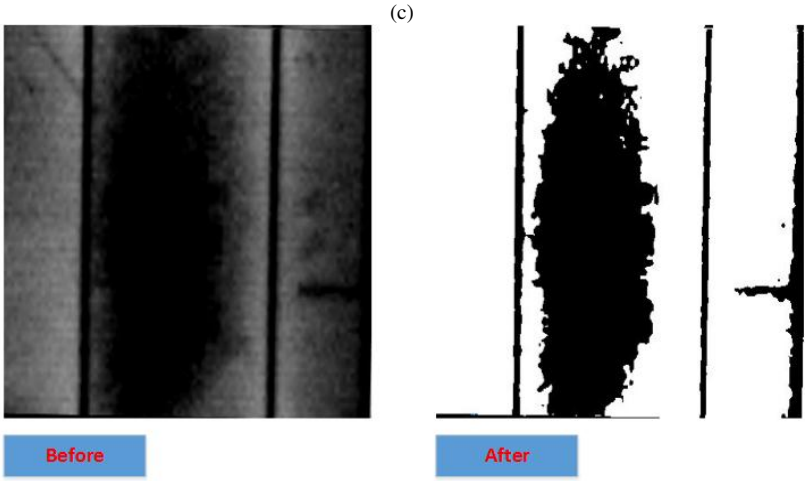

(d)

Fig. 3. (a) bit-by-bit pixel calibration ,(b) Before and after using the proposed OR function, this method uses the OR function between each bit-by-bit of the pixels from the original cracked cell with free crack solar cell, this solar cell is corresponds to sample 1 in the entire manuscript, (c) Solar cell sample 2, (d) Solar cell sample 3

IV. Solar Cell Accept/Reject Criterion

A. General Description

After examining the solar cell using the proposed inspection method discussed earlier in section III, the final calibrated image of the solar cell will be processed using the plot profile method which is well known as the distance in pixels vs. the gray level (the level of the dark spots at specific x-axis distance) [26].

The optimum/ideal plot profile must be known by the micro crack detection system in order to detect possible cracks in the observed solar cell. For that reason, a healthy/none-cracked solar cell is captured and the plot profile using the gray level is measured. The plot profile and the healthy solar cell calibrated image are shown in Fig. 4(a). Using the developed software, all captured images are taken in a resolution of 200 x 200 pixels, therefore, the x-axis in Fig. 4(a) is limited to 200. In addition, the y-axis presents the gray level of the dark spots in the image, where clean/no-cracks positions have the highest gray level.

From this definition, it is evident that the solar cell gray level is equal to 254. Since the image might contain some minor calibration errors or miscalculation of the exact image pixel size, and in order to eliminate this problem, we have set a 10% confidence threshold to the gray level to set up the upper and lower detection limits. These limits are shown in Fig. 4(a) and are equal to 268 and 242, respectively.

An additional problem raised while adjusting the accept/reject criterion that the solar cells contain busbars. To overcome this problem, the examined solar cells were tested, and the distance of the busbars were identified. Consequently, at certain distance/pixel, the gray level would be projected to reduce significantly. As shown in Fig. 4(a), the solar cell busbars have two fundamental intervals: First busbar from 41 to 48 pixel; Second busbar from 153 to 160 pixel.

Therefore, at these distances, the detection algorithm would not consider the drop in the gray level as an indicator for a micro crack existence. Fig. 4(b) shows a cracked solar cell including the output plot profile. There are several micro cracks affecting the solar cell in the left-hand side, practically, by looking at the plot profile, it is evident that area 1 contains a significant drop in the gray level due to the present of a micro cracks. Similarly, after the first solar cell busbar, additional micro cracks appear in the solar cell; labeled as area 2.

Due to the change in the temperature, solar illumination, humidity and other environmental conditions in the manufacturing process of the solar cell, some solar cells might contain negligible micro cracks, but in which they do not reflect to an actual micro crack or damage in the solar cell wafer. For example, Fig. 5 shows a trivial micro crack affecting a solar cell. According to the plot profile, the gray level is always within an accepted level. Hence, the micro cracks labeled in the circle on Fig. 5, do not have a meaningful influence on the gray level of the plot profile. Therefore, the solar cell is accepted and sent to the next stage; the assembling unit.

The scanning for the micro-cracks could be calibrated using a specific solar cell parameter, particular the width size. Since the EL camera identifies the layout of the solar cell, whereby the LabVIEW code is integrated with the specific distances of the busbars. Hence, the developed approach is capable to be attuned based on the specification of the solar cell manufacturing criterion.

It is worth noting that since the proposed method is reliant on the detection of the EL images. Hence, the smallest crack size that could be detected is in a range of 200-700µm; this size is characteristically distinguishable for point, area or line cracks. Depending on the resolution of the EL setup, the smallest crack size might be affected, while in our case we have identified micro cracks such as the point cracks shown in Fig. 4(b) that are typically in a range of 250-350µm, while the size of the area cracks are ranging from 500µm – 5mm.

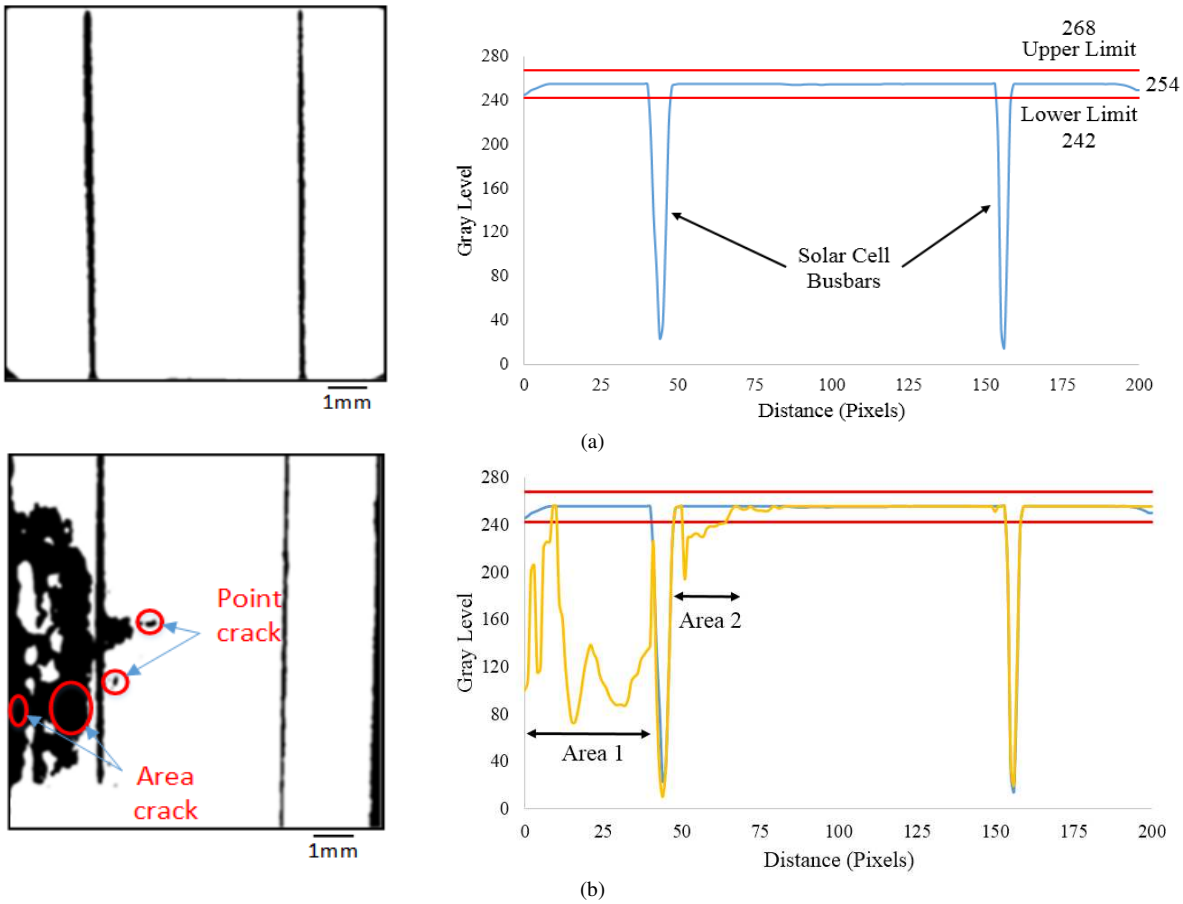

Fig. 4. Solar cell accept/reject plot. (a) Healthy solar cell calibrated image and its plot profile using the gray level, (b) Cracked solar cell and its plot profile

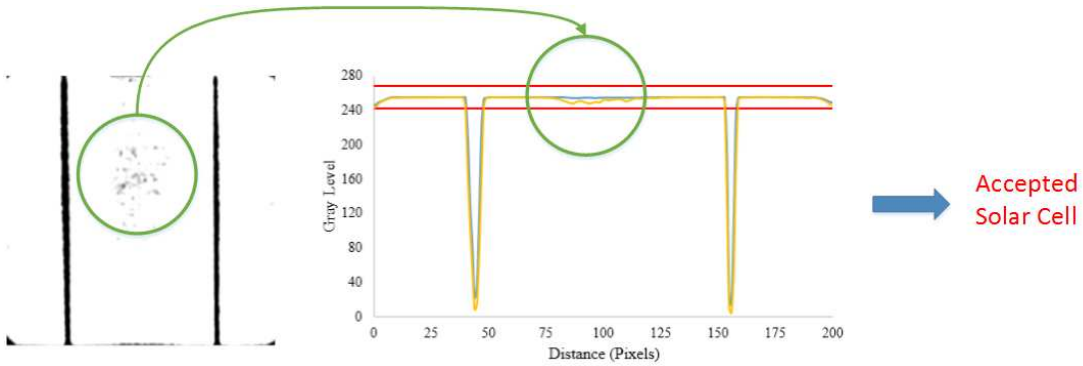

Fig. 5. Example for accepted solar cell with existence of negligible micro cracks,

B. Gray Level Identification Process

The identification of the gray level strongly depends on the image resolution as well as the EL image carrier recombination processes. In this article, we have selected a threshold of 254±10%, since the original EL image is captured for the solar cells powered at their I_{sc} current, which is a common practice for EL imaging system. However, the gray level might change if the solar cell sample is powered up at different current biasing, i.e. at 50% I_{sc} or 75% I_{sc}.

In order to understand the impact of the gray level and the detection of the cracks using different biasing current for a typical EL system, we have examined the same solar cell (healthy/non-cracked) using the proposed method while biasing the cell under three different conditions including I_{sc} current, 75% of I_{sc} and 50% of I_{sc}. The results of the output images are shown in Figs. 6(a-c). It is a well-known phenomenon that while biasing the solar cell under lower rate of its typical Isc, the yielded image of the EL would expect to have noise and the cracks are hardly to determine. This is evident since at 50 and 70% of the I_{sc} the output image does appear to have some micro cracks, while in fact these cracks are not present in the solar cell. The gray level of the three obtained images are measured, while the same threshold of 254±10% is applicable for all the images. However, there is a significant drop in the gray level of the 50% I_{sc} scenario, since at this current biasing level the determined cracks are uncertain; results of the gray level are summarized in Fig. 6(d).

By contrast with above results, the proposed method set a threshold of 254±10% for the gray level for any image obtained using the proposed method. This threshold is fixed since the layout of the yielded image is always having a white background color which is typically emphasized with 254 of gray level.

C. Detection of Micro/Nano Cracks including Different Image Resolution

In this section, the evaluation of the proposed technique using different image resolution and magnification will be presented. We have captured two solar cells images under magnification process of 200 µm, are shown in Fig. 7(a). The detectable image resolution is 300 x 300 pixels; different than the resolution of the images presented earlier in Fig. 4 and Fig. 5 of 200 x 200 pixels. In addition, there is a busbar shown in both observed cells (middle black line across the image). According to the second solar cell, the micro crack is affecting the busbar and adjacent areas.

Both the healthy and the cracked solar cell images are processed using the proposed technique; adjusting the resolution of the calibration mode would result a plot profile that corresponds to the actual resolution of the observed images. The result of the output plot profile is shown in Fig. 7(b), where the maximum x-axis of 300 corresponds to the distance (in pixels), and the gray level is presented on the y-axis. There is a significant difference of the measured gray level for the cracked solar cell compared to the healthy solar cell sample. The drop in the gray level is due to the existence of the cracks in the second captured image.

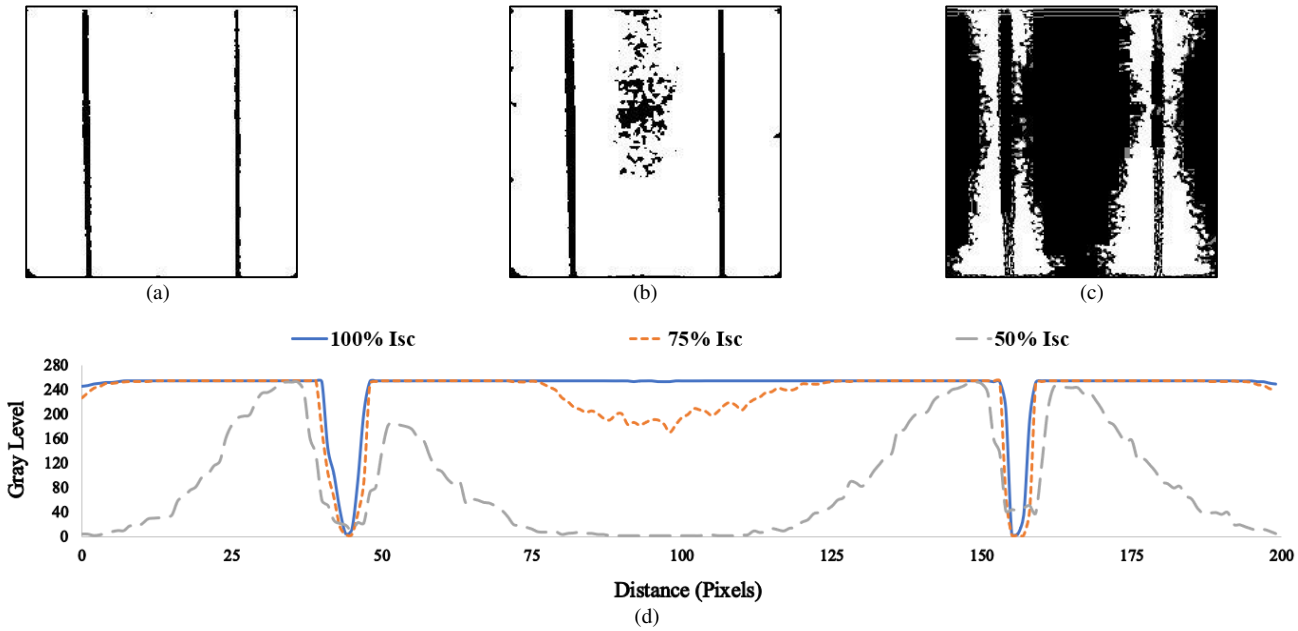

Fig. 6. Healthy solar cell examined under different I_{sc} biasing current. (a) I_{sc}, (b) 75% of I_{sc}, (c) 50% of I_{sc}, (d) Plot profile obtained using all examined I_{sc} thresholds

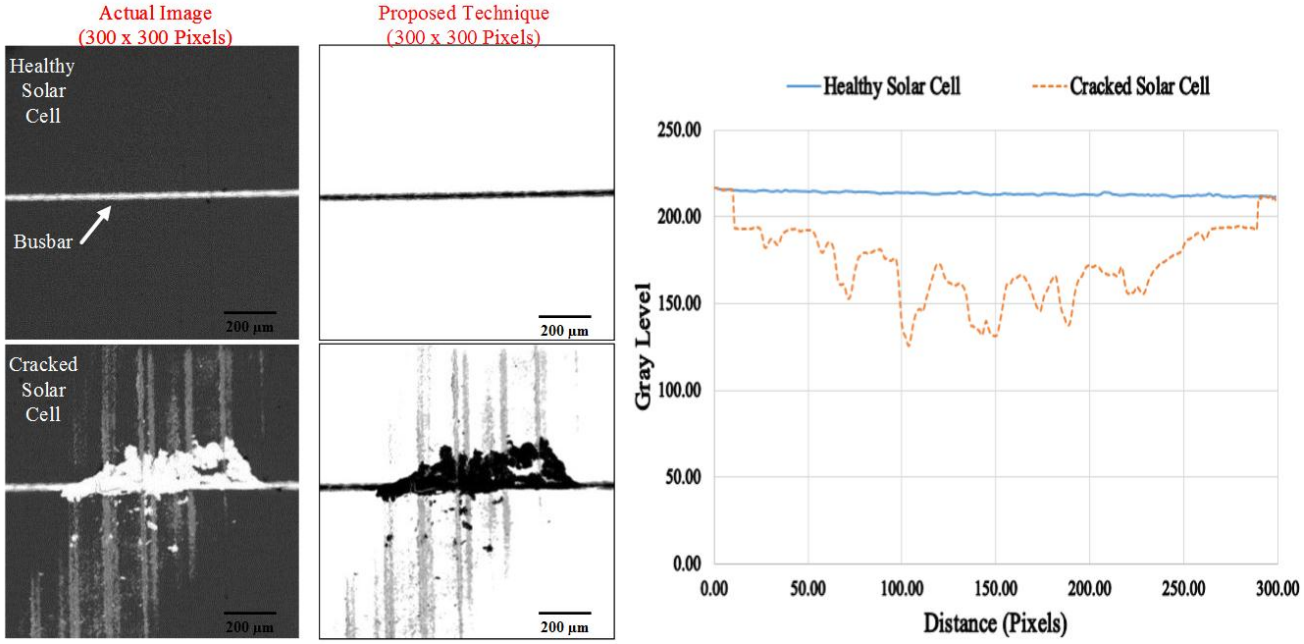

(a) (b)

Fig. 7. (a) Healthy vs. cracked solar cell sample; image resolution: 300 x 300 Pixels, Magnification of 200µm, (b) Output plot profile for both examined solar cell samples

D. Detection of Line Defects, Point Detects, and Crack-Free Solar Cells

In this section, the evaluation of the proposed method using the detection of line defects, point/dot defects and crack-free solar cells will be presented. We have examined a solar cell under an electron microscopy while setting the magnification on 1mm.

The captured image of the electron microscopy is shown in Fig. 8(a). The output image observed using the proposed detection method is shown in Fig. 8(b). It is evident that the line cracks in the busbars are clearly detectible, while a crack-free location of the solar cell are presented by a clear non-blacked-areas. In addition, the point/dot cracks of the examined solar cell are obtained. The only limitation associated with the point cracks that the actual position and orientation are hardly to be acknowledged by the proposed method since this type of the cracks does have minimal effect on the surface/layout of the solar cell and their width commonly less than 250 micron. On the other hand, the proposed method perfectly can detect line cracks within minimal error associated with the yielded image.

According to the minimum cracks size inspection, using the electron microscopy, it is possible to detect cracks as small as 10µm. In Fig. 9 we present three different images of the same solar cell sample taken under different magnification: 100µm, 50µm and 10µm.

E. Proposed Method Limitations

The main drawback of the proposed solar cell imaging technique is that the depth of the crack cannot be identified. The reason behind this limitation is due to the EL camera system which only captures the surface layout (well-known as the length) of the solar cell but cannot identify the width of the cracks. In addition, the user of the proposed method must manually calibrate the detection system in order to adjust the plot profile. Hence, the distance (in pixels) of the final output plot profile is relatively identical to the actual detected image.

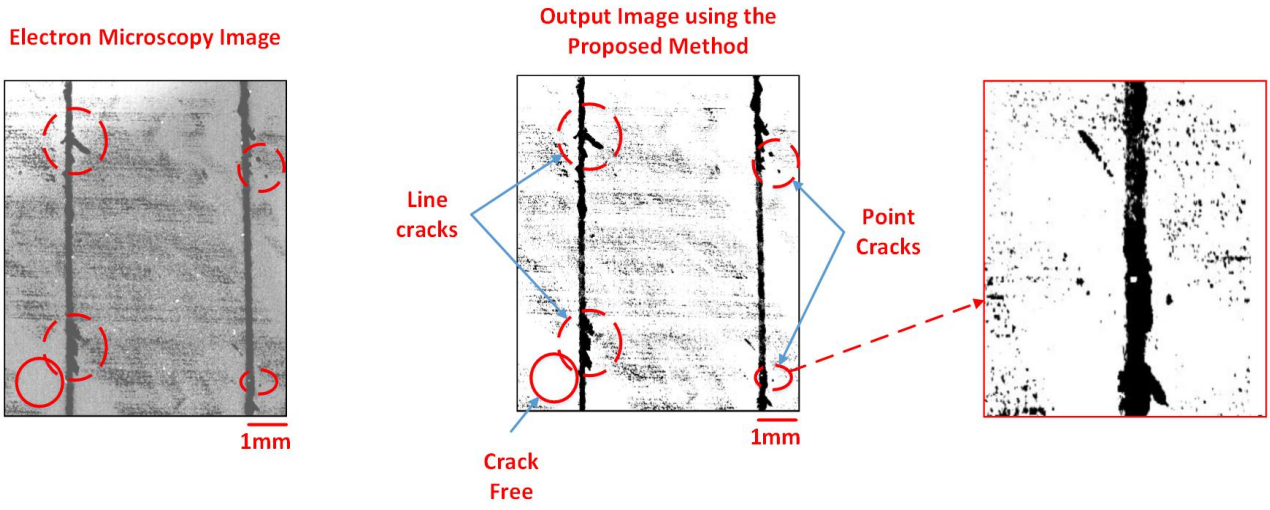

(a) (b)

Fig. 8. Cracked solar cell. (a) Examined under electron microscopy, (b) Output image using the proposed detection method

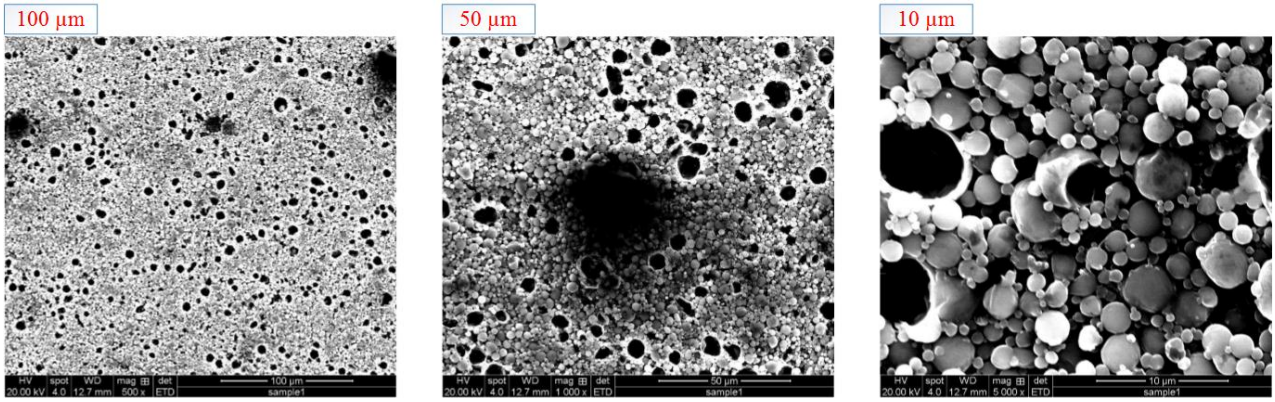

Fig. 9. Micro cracks detection using electron microscopy with different magnification; 100µm - 10 µm

V. Conclusion

This paper presents we have presented a novel solar cell micro crack detection system. The proposed technique is based on a specific process which calculate bit-by-bit image pixels of a conventional EL image, thus to remove the noise and improve the quality and localization of the cracks in a typical solar cell image. The Obtained bits are then processed by an OR function in order to generate the output image of cracks. The final calibrated image attained by the OR function will be processed using the plot profile in order to accept/reject the solar cell during a manufacturing process. We have selected a threshold of 254±10% for the plot profile, since most conventional EL images are captured while the solar cells are powered at their I_{sc} current, this procedure is a common practice for industrial EL imaging system. In order to examine the feasibility of the proposed technique, different cracked solar cells have been examined. Results show that the micro cracks size, orientation, and location is more visible using the proposed technique compared to the conventional EL detection method. Furthermore, the proposed technique has been applied on multiple images captured using electron microscopy that are taken at different magnification and resolution levels.

References

[1] A. Belyaev, O. Polupan, W. Dallas, S. Ostapenko, D. Hess and J. Wohlgemuth, "Crack detection and analyses using resonance ultrasonic vibrations in full-size crystalline silicon wafers," in Applied Physics Letters, vol. 88, no. 11, pp. 111907, Feb. 2006, doi: 10.1063/1.2186393.

[2] S. Ostapenko, U.S. Patent No. 8,528,407, 2013, Washington, DC: U.S. Patent and Trademark Office.

[3] H. Nan, Z. Wang, W. Wang, Z. Liang, Y. Lu, Q. Chen, D. He, P. Tan, F. Miao, X. Wang, J. Wang and Z. N, "Strong photoluminescence enhancement of MoS2 through defect engineering and oxygen bonding," in ACS nano, vol. 8, no. (6), pp. 5738-5745, doi: 10.1021/nn500532f.

[4] Y. Wu, X. Yang, W. Chen, Y. Yue, M. Cai, F. Xie, E. Bi, A. Islam and L. Han, "Perovskite solar cells with 18.21% efficiency and area over 1 cm2 fabricated by heterojunction engineering," in Nature Energy, vol. 1, no. 11, pp. 16148, Sep. 2016, doi: 10.1038/nenergy.2016.148.

[5] Y. Zhu, M. K. Juhl, T. Trupke and Z. Hameiri, "Photoluminescence Imaging of Silicon Wafers and Solar Cells With Spatially Inhomogeneous Illumination," in IEEE Journal of Photovoltaics, vol. 7, no. 4, pp. 1087-1091, July 2017, doi: 10.1109/JPHOTOV.2017.2690875.

[6] R. Bhoopathy, O. Kunz, M. Juhl, T. Trupke and Z. Hameiri, Z, "Outdoor photoluminescence imaging of photovoltaic modules with sunlight excitation," in Progress in Photovoltaics: Research and Applications, vol. 26, no. 1, pp. 69-73, Sep. 2017, doi: 10.1002/pip.2946.

[7] M. Dhimish, V. Holmes, P. Mather, C. Aissa and M. Sibley, "Development of 3D graph-based model to examine photovoltaic micro cracks," in Journal of Science: Advanced Materials and Devices, vol. 3, no. 3, pp. 380-388, Sep. 2018, doi: 10.1016/j.jsamd.2018.07.004.

[8] M. Köntges, M. Siebert, D. Hinken, U. Eitner, K. Bothe and T. Potthof, "Quantitative analysis of PV-modules by electroluminescence images for quality control," in 24th European Photovoltaic Solar Energy Conference, Hamburg, Germany, pp. 21-24, Sep. 2009, doi: 10.4229/24thEUPVSEC2009-4CO.2.3.

[9] T. Fuyuki and A. Kitiyanan, "Photographic diagnosis of crystalline silicon solar cells utilizing electroluminescence," in Applied Physics A, vol. 96, no.1, pp. 189-196, July 2009, doi: 10.1007/s00339-008-4986-0.

[10] M. Dhimish, V. Holmes, M. Dales and B. Mehrdadi, "Effect of micro cracks on photovoltaic output power: case study based on real time long term data measurements," in Micro & Nano Letters, vol. 12, no. 10, pp. 803-807, 10 2017, doi: 10.1049/mnl.2017.0205.

[11] M. Kontgers, I. Kunze, S. Kajari-Schroder, X. Breitenmoser and B. Bjorneklett, "Quantifying the risk of power loss in PV modules due to micro cracks," in 25th European Photovoltaic Solar Energy Conference, Valencia, Spain, pp. 3745-3752, Sep. 2010, doi: 10.4229/25thEUPVSEC2010-4BO.9.4.

[12] S. Kajari-Schröder, I. Kunze, U. Eitner and M. Köntges, "Spatial and orientational distribution of cracks in crystalline photovoltaic modules generated by mechanical load tests," in Solar Energy Materials and Solar Cells, vol. 95, no. 11, pp. 3054-3059, Nov. 2011, doi: 10.1016/j.solmat.2011.06.032.

[13] S. Oh et al., "Control of Crack Formation for the Fabrication of Crack-Free and Self-Isolated High-Efficiency Gallium Arsenide Photovoltaic Cells on Silicon Substrate," in IEEE Journal of Photovoltaics, vol. 6, no. 4, pp. 1031-1035, July 2016, doi: 10.1109/JPHOTOV.2016.2566887.

[14] X. Qian, H. Zhang, C. Yang, Y. Wu, Z. He, Q. E. Wu and H. Zhang, "Micro-cracks detection of multicrystalline solar cell surface based on self-learning features and low-rank matrix recovery," in Sensor Review, vol. 38, no. 3, pp. 360-368, Dec. 2017, doi: 10.1108/SR-08-2017-0166.

[15] Z. Chen, L. Wu, S. Cheng, P. Lin, Y. Wu and W. Lin, "Intelligent fault diagnosis of photovoltaic arrays based on optimized kernel extreme learning machine and IV characteristics," in Applied Energy, vol. 204, pp. 912-931, Oct. 2017, doi: 10.1016/j.apenergy.2017.05.034.

[16] M. Dhimish, P. Mather and V. Holmes, "Evaluating Power Loss and Performance Ratio of Hot-Spotted Photovoltaic Modules," in IEEE Transactions on Electron Devices, vol. 65, no. 12, pp. 5419-5427, Dec. 2018, doi: 10.1109/TED.2018.2877806.

[17] W. S. M. Brooks, D. A. Lamb and S. J. C. Irvine, "IR Reflectance Imaging for Crystalline Si Solar Cell Crack Detection," in IEEE Journal of Photovoltaics, vol. 5, no. 5, pp. 1271-1275, Sept. 2015, doi: 10.1109/JPHOTOV.2015.2438636.

[18] M. Dhimish, V. Holmes, B. Mehrdadi and M. Dales, "The impact of cracks on photovoltaic power performance," in Journal of Science: Advanced Materials and Devices, vol. 2, no. 2, pp. 199-209, June 2017, doi: 10.1016/j.jsamd.2017.05.005.

[19] A. Bar-Zion, C. Tremblay-Darveau, O. Solomon, D. Adam and Y. C. Eldar, "Fast Vascular Ultrasound Imaging With Enhanced Spatial Resolution and Background Rejection," in IEEE Transactions on Medical Imaging, vol. 36, no. 1, pp. 169-180, Jan. 2017, doi: 10.1109/TMI.2016.2600372.

[20] K. Zhang, D. Tao, X. Gao, X. Li and Z. Xiong, "Learning Multiple Linear Mappings for Efficient Single Image Super-Resolution," in IEEE Transactions on Image Processing, vol. 24, no. 3, pp. 846-861, March 2015, doi: 10.1109/TIP.2015.2389629.

[21] A. Dolara, G. C. Lazaroiu, S. Leva, G. Manzolini and L. Votta, "Snail Trails and Cell Microcrack Impact on PV Module Maximum Power and Energy Production," in IEEE Journal of Photovoltaics, vol. 6, no. 5, pp. 1269-1277, Sept. 2016, doi: 10.1109/JPHOTOV.2016.2576682.

[22] A. A. Y. Mustafa, "Probabilistic binary similarity distance for quick binary image matching," in IET Image Processing, vol. 12, no. 10, pp. 1844-1856, 10 2018, doi: 10.1049/iet-ipr.2017.1333.

[23] M. Dhimish, V. Holmes, B. Mehrdadi, M. Dales and P. Mather, "Output-Power Enhancement for Hot Spotted Polycrystalline Photovoltaic Solar Cells," in IEEE Transactions on Device and Materials Reliability, vol. 18, no. 1, pp. 37-45, March 2018, doi: 10.1109/TDMR.2017.2780224.

[24] J. Song, H. Zhang, X. Li, L. Gao, M. Wang and R. Hong, "Self-Supervised Video Hashing With Hierarchical Binary Auto-Encoder," in IEEE Transactions on Image Processing, vol. 27, no. 7, pp. 3210-3221, July 2018, doi: 10.1109/TIP.2018.2814344.

[25] M. Dhimish, "Assessing MPPT Techniques on Hot-Spotted and Partially Shaded Photovoltaic Modules: Comprehensive Review Based on Experimental Data," in IEEE Transactions on Electron Devices, vol. 66, no. 3, pp. 1132-1144, March 2019, doi: 10.1109/TED.2019.2894009.

[26] M. Dhimish, V. Holmes and P. Mather, "Novel Photovoltaic Micro Crack Detection Technique," in IEEE Transactions on Device and Materials Reliability, doi: 10.1109/TDMR.2019.2907019.